

Thermodynamic Optimization of Ca-Fe-Si System and Its Applications to Metallurgical Grade Si-Refining Process

SENLIN CUI, MANAS PALIWAL, and IN-HO JUNG

Thermodynamic optimization of the binary Ca-Fe and ternary Ca-Fe-Si systems has been conducted based on the critical evaluation of all phase diagram and thermodynamic properties data available in the literature. The thermodynamics of the liquid solution was described using the Modified Quasichemical Model which takes into account short-range ordering. As a result, a set of model parameters for all solid and liquid phases was produced. With the help of a Gibbs energy minimization routine, any thermodynamic properties and phase diagrams in the ternary system can be calculated. Several pseudo-binary sections and isopleths in the ternary Ca-Fe-Si system were predicted from the present thermodynamic model with optimized model parameters. In addition, Scheil cooling calculations were performed to understand the evolution of as-cast microstructure of metallurgical grade Si (Si-Fe-Ca alloy) depending on its impurity content.

DOI: 10.1007/s40553-014-0010-0

© The Minerals, Metals & Materials Society and ASM International 2014

I. INTRODUCTION

IN order to understand and optimize the complex chemical reactions during refining of metallurgical grade silicon (MG-Si) and understand the evolution of Si alloy microstructure in various applications, knowledge of the phase diagram and thermodynamic properties of Si alloy is critical. Unfortunately, such information is still lacking in the literature. Recently, Tang *et al.*^[1] collected all the phase diagram data and thermodynamic information of a wide range of impurity elements for MG-Si and evaluated the thermodynamic parameters to reproduce the impurity behavior in the Si-rich region. Such information is critical to understand impurity segregation between solid Si and liquid Si during solidification and the reactivity with molten slag for slag-refining processes.

Fe and Ti in molten Si are typically difficult to remove during the slag-refining process;^[2] therefore, alternative acid-leaching processing routes were proposed to eliminate these elements. In the acid-leaching process, the evolution of the as-cast microstructure, and more specifically the evolution of Fe and Ti intermetallic precipitates in solidified Si, is important to determine the removal rate of Fe and Ti. Consequently, accurate phase diagram information is necessary not only for Si-rich compositions but also for a wide range of ternary and higher order Si-containing systems.

In the case of Fe removal by the acid-leaching process, Si-Ca-Fe ternary alloys can be considered. In order to maximize Fe removal, proper amounts of Ca

can be intentionally added to Fe (Ca can also be dissolved from molten CaO-containing slag during the slag treatment). According to the study of Sakata *et al.*,^[3] the control of the Ca/Fe ratio in liquid Si is a key factor in Fe removal during the subsequent acid-leaching process. In order to understand the evolution of the microstructure during solidification of the Si-Ca-Fe system, the phase diagram of the Ca-Fe-Si system is thus needed. Unfortunately, no accurate information on the phase diagram is available in the literature.

The CALPHAD technique is very efficient to perform the thermodynamic assessment (optimization or modeling) of complex systems with limited thermodynamic and phase diagram data. The thermodynamic assessment of the ternary Ca-Fe-Si system was performed previously by Anglézio *et al.*^[4] They also carried out assessments of the binary Ca-Si and Ca-Fe systems. Unfortunately, the available information for the binary Ca-Fe system was not well taken into account and the description of ternary Ca-Fe-Si system was not satisfactory. A new thermodynamic optimization of the ternary Ca-Fe-Si system is thus suitable.

The purpose of the present study is to optimize thermodynamically the binary Ca-Fe and ternary Ca-Fe-Si systems. Based on the critical evaluation of all thermodynamic properties and phase diagram data from the literature, thermodynamic model parameters, which can simultaneously reproduce all reliable experimental data, were obtained. Our binary model parameters for the Ca-Fe system were combined with previous binary model parameters for the Ca-Si and Fe-Si systems to develop the thermodynamic database of the ternary Ca-Fe-Si system. All the experimental data of the ternary system were taken into account to produce the best thermodynamic database. Using this newly developed database, many unexplored phase diagram and liquidus projections of the ternary system were calculated. In addition, Scheil cooling calculations of Si-rich alloys containing Ca and Fe impurities were performed to

SENLIN CUI and MANAS PALIWAL, Graduate Students, and IN-HO JUNG, Associate Professor, are with the Department of Mining and Materials Engineering, McGill University, 3610 University, Montreal, QC H3A 0C5, Canada. Contact e-mail: in-ho.jung@mcgill.ca

Manuscript submitted November 5, 2013.

Article published online February 11, 2014

understand the evolution of the as-cast microstructures. This information can be helpful to understand Fe removal in acid-leaching processes. All thermodynamic calculations were performed using the FactSage software.^[5]

II. THERMODYNAMIC MODELS

In the thermodynamic “optimization” of a chemical system, all available thermodynamic and phase equilibrium data are evaluated simultaneously in order to obtain a set of model equations for the Gibbs energies of all phases as functions of temperature and composition. From these equations, all the thermodynamic properties and phase diagrams can be back-calculated. In this way, all the data are rendered self-consistent and consistent with thermodynamic principles. Thermodynamic property data, such as activity data, can aid in the evaluation of the phase diagram, and phase diagram measurements can be used to deduce thermodynamic properties. Discrepancies in the available data can often be resolved, and interpolations and extrapolations can be made in a thermodynamically correct manner.

A. Stoichiometric Compounds and Elements

The Gibbs energies of all pure elements are taken from SGTE database version 5.0 (2009). The Gibbs energies of stoichiometric compounds were optimized based on available thermodynamic data using the standard Gibbs energy expression based on the heat capacity, enthalpy, and entropy of formation at 298 K (25 °C). Stoichiometric phases exhibiting magnetic transitions associated with Neel or Curie temperatures were described by an empirical relationship suggested by Inden^[6] and modified by Hillert and Jarl.^[7]

The Gibbs energies of pure elements and stoichiometric compounds can be described by

$$G_T^\circ = H_T^\circ - TS_T^\circ, \quad [1]$$

$$H_T^\circ = \Delta H_{298K}^\circ + \int_{T=298K}^T C_p dT, \quad [2]$$

$$S_T^\circ = S_{298K}^\circ + \int_{T=298K}^T (C_p/T) dT, \quad [3]$$

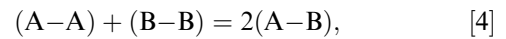
where ΔH_{298K}° is the enthalpy of formation of a given species from pure elements [ΔH_{298K}° of element stable at 298 K (25 °C) and 1 atm is assumed as 0 J/mol; reference state], S_{298K}° is the entropy at 298 K (25 °C), and C_p is the heat capacity.

B. Liquid Phase

In order to take into account the strong ordering tendency of the liquid phase, the Modified Quasichem-

ical Model,^[8,9] which accounts for short-range ordering (SRO) of nearest-neighbor atoms, was used for the liquid solutions. For example, the enthalpy and Gibbs energy of binary Ca-Si liquid shows a very negative deviations from ideal solution, which indicates a strong SRO in the liquid solution. The enthalpy of mixing of the Ca-Si liquid solution is as negative as -40 kJ/g-atom.^[10] A similar negative enthalpy of mixing can be observed for the liquid Fe-Si solution.^[11] The Modified Quasichemical Model can give a more realistic thermodynamic description for liquid solutions, compared with the conventional simple random-mixing Bragg Williams model. The Modified Quasichemical Model has been successfully applied to many liquid metallic solutions^[8,12,13] and ionic solutions^[14,15] exhibiting strong SRO behavior. A short description of the model is given below. Details about the model can be found in previous studies.^[8,9]

Let us consider the case of a binary A–B liquid solution. The atoms A and B are distributed over the sites of a quasi-lattice in a liquid solution. The following pair exchange reaction can be considered:



where (A–B) represents a first-nearest-neighbor pair of A and B. The non-configurational Gibbs energy change for the formation of two moles of (A–B) pairs according to reaction^[16] is Δg_{AB} . Then, the Gibbs energy of the solution is given by

$$G = (n_A G_A^\circ + n_B G_B^\circ) - T\Delta S^{\text{config}} + n_{AB} \frac{\Delta g_{AB}}{2}, \quad [5]$$

where G_A° and G_B° are the molar Gibbs energies of the pure components A and B, n_A and n_B are the numbers of moles of A and B atoms, and n_{AB} is the number of moles of (A–B) pairs. ΔS^{config} is the configurational entropy of mixing given by a random distribution of the (A–A), (B–B), and (A–B) pairs in the one-dimensional Ising approximation:

$$\begin{aligned} \Delta S^{\text{config}} = & -R(n_A \ln X_A + n_B \ln X_B) \\ & - R \left[n_{AA} \ln \left(\frac{X_{AA}}{Y_A^2} \right) + n_{BB} \ln \left(\frac{X_{BB}}{Y_B^2} \right) \right. \\ & \left. + n_{AB} \ln \left(\frac{X_{AB}}{2Y_A Y_B} \right) \right], \end{aligned} \quad [6]$$

where n_{AA} , n_{BB} , and n_{AB} are the numbers of moles of each kind of pairs. The pair fractions (X_{AA} , X_{BB} , and X_{AB}) and coordination equivalent fractions (Y_A and Y_B) can be calculated as

$$X_{AA} = \frac{n_{AA}}{n_{AA} + n_{BB} + n_{AB}}, \quad [7]$$

$$X_{BB} = \frac{n_{BB}}{n_{AA} + n_{BB} + n_{AB}}, \quad [8]$$

$$X_{AB} = \frac{n_{AB}}{n_{AA} + n_{BB} + n_{AB}}, \quad [9]$$

$$Y_A = X_{AA} + \frac{1}{2}X_{AB}, \quad [10]$$

$$Y_B = X_{BB} + \frac{1}{2}X_{AB}. \quad [11]$$

The Δg_{AB} term is the model parameter to reproduce the Gibbs energy of the liquid phase of the binary A–B system, which is expanded as a polynomial in terms of the pair fractions, as follows:

$$\Delta g_{AB} = \Delta g_{AB}^{\circ} + \sum_{i \geq 1} g_{AB}^{i\circ} (X_{AA})^i + \sum_{j \geq 1} g_{AB}^{j\circ} (X_{BB})^j, \quad [12]$$

where Δg_{AB}° , $g_{AB}^{i\circ}$, and $g_{AB}^{j\circ}$ are the adjustable model parameters which can be functions of temperature.

In the Modified Quasichemical Model, the coordination numbers of A and B, Z_A and Z_B , can now be varied with composition to reproduce the SRO as follows:

$$\frac{1}{Z_A} = \frac{1}{Z_{AA}} \left(\frac{2n_{AA}}{2n_{AA} + n_{AB}} \right) + \frac{1}{Z_{AB}} \left(\frac{n_{AB}}{2n_{AA} + n_{AB}} \right), \quad [13]$$

$$\frac{1}{Z_B} = \frac{1}{Z_{BB}} \left(\frac{2n_{BB}}{2n_{BB} + n_{AB}} \right) + \frac{1}{Z_{BA}} \left(\frac{n_{AB}}{2n_{BB} + n_{AB}} \right), \quad [14]$$

where Z_{AA} is the value of Z_A when all nearest neighbors of an A atom are A atoms, and Z_{AB} is the value of Z_A when all nearest neighbors are B atoms. Z_{BB} and Z_{BA} are defined in an analogous manner. In the present study, Z_{ii} for all elements ($i = \text{Ca, Si, or Fe}$) are set to be 6. As the maximum ordering of all binary systems happens at AB composition, $Z_{AB} = Z_{BA}$ (6 for Fe-Si and Ca-Fe system and 4 for Ca-Si system).

The Gibbs energy of the liquid phase in the ternary system can be calculated by interpolating binary parameters. Different interpolation techniques can be used based on the nature of the ternary system. If the interpolated Gibbs energy of a ternary liquid phase is not sufficient to reproduce the phase diagram and thermodynamic properties of the ternary liquid phase, small ternary model parameters can be introduced into the models to resolve remaining disagreements with available experimental data. As the liquid phases of the binary Ca-Si and Fe-Si systems show very negative but similar deviation from ideal solution and the Ca-Fe system shows positive deviation from ideal solution, the Toop-type interpolation technique with Si as the asymmetric component is chosen as the proper interpolation technique. The details of the interpolation method can be found elsewhere.^[17]

C. Solid Solutions

There are several solid solutions in the ternary system:

- (i) Diamond_A4 phase: Si-rich solid solution phase dissolving very dilute amounts of Fe and Ca.
- (ii) FCC_A1 phase: fcc-Fe phase with significant solubility of Si and minor solubility of Ca.
- (iii) BCC_A2 phase: bcc-Fe phase with significant solubility of Si and minor solubility of Ca, and

Ca-rich solid solution with small solubility of Fe. Miscibility gap between Fe-rich and Ca-rich solid solution.

- (iv) Ordered BCC phases: two types of ordered bcc-Fe phases in the Fe-Si system.

The Gibbs energy of solid solutions was described with the Compound Energy Formalism^[18] according to their crystal structure. Among them, the Si-rich Diamond_A4 solution was described by assuming that Fe and Ca are dissolving into solid Si by replacing Si in substitutional sites. The molar Gibbs energy of the solid solution can be expressed as

$$\begin{aligned} G = & (y_{\text{Si}}G_{\text{Si}}^{\circ} + y_{\text{Fe}}G_{\text{Fe}}^{\circ} + y_{\text{Ca}}G_{\text{Ca}}^{\circ}) \\ & + RT(y_{\text{Si}} \ln y_{\text{Si}} + y_{\text{Fe}} \ln y_{\text{Fe}} + y_{\text{Ca}} \ln y_{\text{Ca}}) \\ & + {}^aL_{\text{Si,Fe}}y_{\text{Si}}y_{\text{Fe}}(y_{\text{Fe}} - y_{\text{Si}})^a \\ & + {}^aL_{\text{Si,Ca}}y_{\text{Si}}y_{\text{Ca}}(y_{\text{Ca}} - y_{\text{Si}})^a \\ & + {}^aL_{\text{Ca,Fe}}y_{\text{Ca}}y_{\text{Fe}}(y_{\text{Fe}} - y_{\text{Ca}})^a, \end{aligned} \quad [15]$$

where y_i is the site fractions of i in the sublattice, and R and T are the gas constant and temperature in Kelvin. G_{Si}° is the molar Gibbs energy of solid Si, and G_{Ca}° and G_{Fe}° are the pseudo-molar Gibbs energies of solid Ca and Fe in the Diamond-A4 structure. The binary interaction parameters between Si and solutes (Ca and Fe) in the sublattice, ${}^aL_{\text{Si,Ca}}$, ${}^aL_{\text{Si,Fe}}$, and ${}^aL_{\text{Ca,Fe}}$ where $a \geq 0$, are adjustable model parameters to reproduce the solubilities of Ca and Fe in solid Si in binary systems.

Other solid solutions were described in similar manner.

III. RESULTS OF THERMODYNAMIC OPTIMIZATION

All thermodynamic data and phase diagram data in the binaries and ternary systems were collected from literature and evaluated together to find out the inconsistencies between the experimental data. Then, the optimized model parameters for the thermodynamic models were obtained to simultaneously reproduce all the reliable experimental data. The details of the thermodynamic optimization of each system are presented below and all optimized model parameters obtained in the present study are listed in Table I.

A. Binary Systems

1. The Ca-Si system

All thermodynamic properties and the phase diagram of the binary Ca-Si system were well optimized by Heyrman and Chartrand.^[10] They effectively resolved the inconsistency in the solid enthalpy of formations data from the well-optimized thermodynamic properties of the liquid using the Modified Quasichemical Model. Figure 1 shows the calculated phase diagram of the Ca-Si system from the optimized model parameters by Heyrman and Chartrand.

Their thermodynamic model parameters were used in the present study without any modification. The only

Table I. Thermodynamic Model Parameters for the Ca-Fe-Si System Optimized in the Present Study (J mol⁻¹ or J mol⁻¹ K⁻¹)

Phase	Thermodynamic Parameters
Liquid	$\Delta g_{\text{Fe,Ca}} = 40584.8 - 3.72376T - 5439.2X_{\text{Ca,Ca}} + 6276X_{\text{Fe,Fe}}$ $\Delta g_{\text{Fe,Si}} = -33710.488 + 2.25936T + (-12552 + 5.0208T)X_{\text{Fe,Fe}} + (-8368 + 4.8116T)X_{\text{Fe,Fe}}^2$ $+ (-3054.32 + 6.4852T)X_{\text{Si,Si}}$ $\Delta g_{\text{Ca,Si}} = -47279.2 + 1.8828T + (-17991.2)X_{\text{Si,Si}} + (-1354.3 - 16.7360T)X_{\text{Ca,Ca}}$ $W_{\text{Fe,Si,(Ca)}}^{001} = -10920.2$ $W_{\text{Ca,Si,(Fe)}}^{001} = 15104.2$
Fcc	${}^0L_{\text{Fe,Ca}} = 106897.81096$ ${}^0L_{\text{Fe,Si}} = -115254.045552 - 2.19316276032T$ ${}^1L_{\text{Fe,Si}} = -84776.910912 + 44.33086072T$ ${}^2L_{\text{Fe,Si}} = 20007.028188$ ${}^0L_{\text{Ca,Si}} = -62760$
Bcc	${}^0L_{\text{Fe,Ca}} = 110663.41096$ ${}^0L_{\text{Fe,Si}} = -154013.558816 + 32.2895459528T$ ${}^1L_{\text{Fe,Si}} = -63511.471504 + 13.2510945184T$ ${}^2L_{\text{Fe,Si}} = 35727.5789192$ ${}^0L_{\text{Ca,Si}} = 80T$
Hcp	${}^0L_{\text{Fe,Ca}} = 418400$
Diamond	$G_{\text{Ca(Diamond)}}^{\circ} = G_{\text{Ca,fcc}}^{\circ} + 1000$ $G_{\text{Fe(Diamond)}}^{\circ} = G_{\text{Fe,fcc}}^{\circ} + 1000$ ${}^0L_{\text{Ca,Si}} = -2092$ ${}^0L_{\text{Fe,Si}} = 117152$ ${}^0L_{\text{Ca,Fe}} = 209200$
Fe ₂ Si	$\Delta H_{298}^{\circ} = -53889.7, S_{298}^{\circ} = 106.4$ $C_p = 2C_p(\text{Fe}_{\text{(bcc)}}) + C_p(\text{Si}_{\text{(diamond)}})$
Fe ₅ Si ₃	$\Delta H_{298}^{\circ} = -234740, S_{298}^{\circ} = 209.1$ $C_p = 180.30693 + 8.591194310^{-2}T - 1060721.6T^{-2} + 2.664594210^{-7}T^2$ Magnetic moment = 2.32, Curie temperature = 360 K, P factor = 0.28
FeSi	$\Delta H_{298}^{\circ} = -76410, S_{298}^{\circ} = 46.024$ $C_p = 48.56656315 + 1.4721123510^{-2}T - 428219.9934T^{-2} - 1.75113466910^{-6}T^2$
FeSi ₂	$\Delta H_{298}^{\circ} = -96940.44, S_{298}^{\circ} = 55.48$ $C_p = 79.0298507 - 1.81469210^{-2}T - 999009.042T^{-2} + 1.78210^{-5}T^2$
Fe ₃ Si ₇	$\Delta H_{298}^{\circ} = -247842.4242, S_{298}^{\circ} = 207.3$ $C_p = 214.2176 + 1.099271310^{-1}T - 2345706.9T^{-2} - 2.303343410^{-5}T^2$
CaSi	$\Delta H_{298}^{\circ} = -87000.087, S_{298}^{\circ} = 60.428662$ $298 \leq T \leq 716$ $C_p = 57.107853 - 0.010639392T - 474490T^{-2} + 2.702261410^{-5}T^2$ $716 \leq T \leq 1687$ $C_p = 44.941273 + 0.025355808T - 353334T^{-2} + 2.131210^{-8}T^2$ $1687 \leq T \leq 2000$ $C_p = 44.007128 + 0.025871666T$ $2001 \leq T$ $C_p = 95.750461$
CaSi ₂	$\Delta H_{298}^{\circ} = -93724.446, S_{298}^{\circ} = 77.286$ $298 \leq T \leq 716$ $C_p = 82.851606 - 0.006813584T - 827824T^{-2} + 2.704392610^{-5}T^2$ $716 \leq T \leq 1687$ $C_p = 70.685026 + 0.029181616T - 706668T^{-2} + 4.262410^{-8}T^2$ $1687 \leq T \leq 2000$ $C_p = 68.816736 + 0.030213334T$ $2001 \leq T$ $C_p = 129.2434$
Ca ₂ Si	$\Delta H_{298}^{\circ} = -141227.2, S_{298}^{\circ} = 93.256214$ $298 \leq T \leq 716$ $C_p = 85.360953 - 0.025104592T - 595646T^{-2} + 5.402391610^{-5}T^2$ $716 \leq T \leq 1687$ $C_p = 61.027793 + 0.046885808T - 353334T^{-2} + 2.131210^{-8}T^2$ $1687 \leq T \leq 2000$ $C_p = 60.093648 + 0.047401666T$ $2001 \leq T$ $C_p = 154.89698$
Ca ₃ Si ₄	$\Delta H_{298}^{\circ} = -282534.73, S_{298}^{\circ} = 185.858$ $298 \leq T \leq 716$ $C_p = 200.17631 - 0.028092368T - 1776804T^{-2} + 8.108915410^{-5}T^2$ $716 \leq T \leq 1687$ $C_p = 163.67657 + 0.079893232T - 1413336T^{-2} + 8.524810^{-8}T^2$ $1687 \leq T \leq 2000$ $C_p = 159.93999 + 0.081956666T$ $2001 \leq T$ $C_p = 323.85333$
Ca ₅ Si ₃	$\Delta H_{298}^{\circ} = -393521.42, S_{298}^{\circ} = 231.43$ $298 \leq T \leq 716$ $C_p = 227.82976 - 0.060848576T - 1665782T^{-2} + 0.00013507045T^2$ $716 \leq T \leq 1687$ $C_p = 166.99686 + 0.11912742T - 1060002T^{-2} + 6.393610^{-8}T^2$ $1687 \leq T \leq 2000$ $C_p = 164.19442 + 0.120675T$ $2001 \leq T$ $C_p = 405.54442$

Table I. continued

Phase	Thermodynamic Parameters
$\text{Ca}_{14}\text{Si}_{19}$	$\Delta H_{298}^{\circ} = -1275855.9, S_{298}^{\circ} = 912.004$
$298 \leq T \leq 716$	$C_p = 942.22071 - 0.12982245 T - 8409530 T^{-2} + 0.00037842316 T^2$
$716 \leq T \leq 1687$	$C_p = 771.88859 + 0.37411036 T - 6713346 T^{-2} + 4.04928 \cdot 10^{-7} T^2$
$1687 \leq T \leq 2000$	$C_p = 754.13983 + 0.38391166 T$
$2001 \leq T$	$C_p = 1521.9632$

Gibbs energies of all pure elements were taken from SGTE database 5.0.

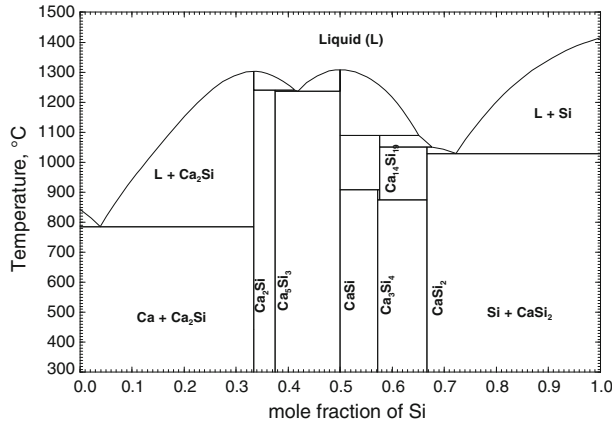


Fig. 1—Calculated phase diagram of the Ca-Si system from the optimization of Heyrman and Chartrand^[10].

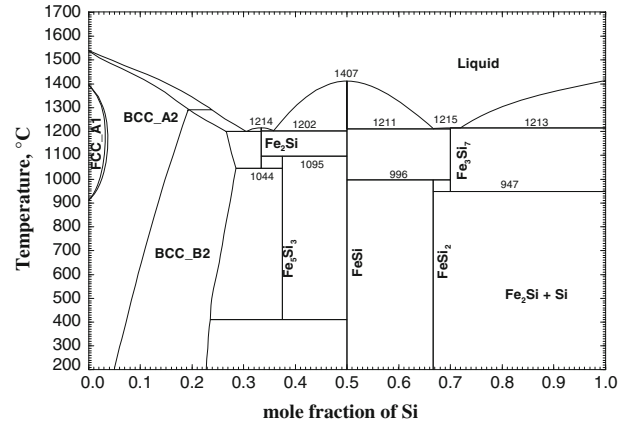


Fig. 3—Calculated phase diagram of the Fe-Si system from the optimization of Cui and Jung^[11].

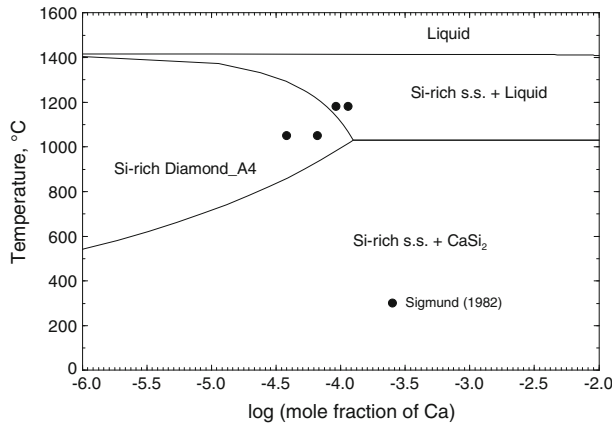


Fig. 2—Optimized solubility of Ca in Si (Diamond_A4) from the present study along with experimental data.

addition in the present study is the description of Ca solubility in solid Si diamond-A4 phase. Heyrman and Chartrand neglected the solubility of Ca in Si because it is less than 1.6×10^{-4} in molar fraction at 1373 K (1100 °C).^[19] However, this is important in the present study for the Si-refining process. Figure 2 shows the solubility of Ca optimized in the present study with experimental data. It should be noted that Sigmund^[19] confirmed that Ca is mainly dissolved on substitutional lattice sites of Si, as we assumed in the present model. In order to describe the solubility, one temperature-independent parameter, ${}^0L_{\text{Si,Ca}}$, was required.

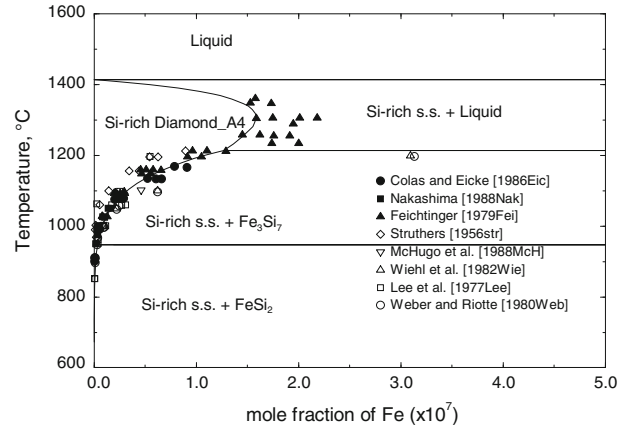


Fig. 4—Optimized solubility of Fe in Si (Diamond_A4) from the present study along with experimental data.

2. The Fe-Si system

This system has been assessed several times. Among them, the assessment by Lacaze and Sundman^[20] is well accepted. However, the reproduction of thermodynamic properties of stoichiometric compounds was less satisfactory. So, the present authors^[11] recently re-optimized the Fe-Si system to reproduce all the thermodynamic and phase diagram data of the Fe-Si system. In particular, the liquid Fe-Si solution was described using the Modified Quasichemical Model, which allows the reproduction of the Gibbs energy of liquid phase accurately. The thermodynamic property data of

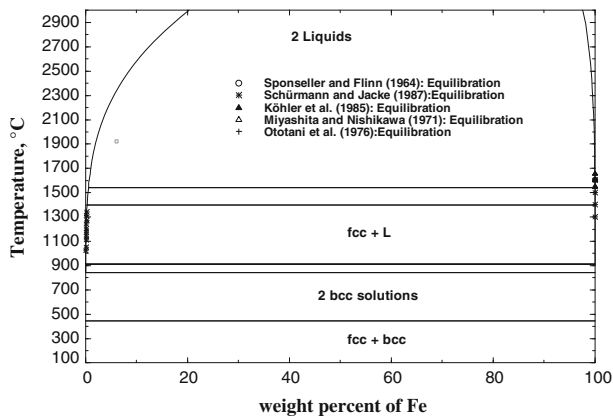


Fig. 5—Calculated phase diagram of the Ca-Fe system from the present study.

stoichiometric solid phases as well as the phase diagram data of the Fe-Si system were well reproduced. The details of new optimization of Fe-Si system will be published elsewhere.^[11] It should be also noted that Tang and Tangstad^[21] performed very careful assessment on Si-rich side of Fe-Si system for high-purity Si application.

The optimized phase diagram is calculated in Figure 3. The calculated solubility of Fe in solid Si is presented in Figure 4 along with associated experimental data. Experimental information on the solubility of Fe in solid silicon was reviewed by Istratov *et al.*^[22] and optimized previously by Tang *et al.*^[1] All experimental data (by Trumbore,^[23] Feichtinger,^[24] and Lee *et al.*^[25] Mchugo *et al.*,^[26] Colas and Weber,^[27] Struthers,^[28] Nakashima *et al.*,^[29] and Gills *et al.*^[30]) except for those from Weber and Riotte^[31] and Wiehl *et al.*^[32] are consistent with each other. The experimental solubility by Weber and Riotte^[31] and Wiehl *et al.*^[32] are larger than other data. In order to reproduce the experimental data, the excess interaction parameter between Si and Fe in the diamond_A4 solution was optimized. A large positive interaction parameter was required.

3. The Ca-Fe system

Large miscibility gaps in both liquid and solid (fcc and bcc solutions) exist in the Ca-Fe system and no intermediate compounds were reported. The solubility of Fe in liquid Ca was only measured by Schürmann and Jacke^[33] from 1293 K to 1703 K (1020 °C to 1430 °C) *via* equilibration experiment. They also reported the solubility of Ca in solid and liquid Fe up to 1873 K (1600 °C). Sponseller and Flinn^[34] determined the solubility of Ca in liquid Fe in sintered TiN crucible to be 0.032 wt pct at 1880 K (1607 °C) under 4 atm Ar pressure. The solubility (0.024 wt pct) of Ca in liquid Fe contained in CaO crucible at 1873 K (1600 °C) under 1 atm Ar gas was reported by Ototani and Kataura.^[35] Miyashita and Nishikawa^[36] determined the Ca concentration in molten liquid at 1873 K (1600 °C) to be at least 0.0103 wt pct Ca, which is smaller than other reported data. Köhler *et al.*^[37] measured Ca solubility in liquid Fe contained in CaO crucible to be about 0.03 wt pct from 1823 K to 1923 K (1550 °C to

1650 °C) using a high-pressure (10 atm Ar pressure) induction furnace and reported that the solubility increased slightly with temperature. The phase diagram studies of the Ca-Fe system were also reviewed by Okamoto.^[38]

Based on the available experimental data, the model parameters for both solid solutions (bcc and fcc solutions) and liquid phase were optimized to reproduce the phase diagram data. The optimized phase diagram is calculated in Figure 5. The magnified views of Ca-rich and Fe-rich regions are presented in Figure 6. The model parameters for solid solutions were determined based on the experimental data of Schürmann and Jacke.^[33] All experimental studies for the solubility of Ca in liquid Fe are consistent with each other except Miyashita and Nishikawa.^[36] During the evaluation of the experimental data, it was found that the miscibility gap (for example, the solubility of Ca in liquid Fe) is insensitive with total pressure up to 10 atm, so all the experimental data can be used in the optimization of the model parameters. It should be noted that the model parameters for solid fcc and bcc Ca-Fe solutions are very similar to each other and symmetric, and the miscibility gap in liquid solution has an asymmetric shape as clearly seen in Figure 5. In comparison to the present study, the previous assessment by Anglézio *et al.*^[4] used only one symmetric excess parameter to reproduce liquid miscibility gap, which cannot reproduce the Fe solubility in the Ca-rich side.

B. Ternary Ca-Fe-Si System

The phase diagram of the Ca-Fe-Si system has not been well studied yet. Neither the subsolidus phase stability of the Ca-Fe-Si system nor thermodynamic properties of liquid solution have been investigated. As mentioned earlier in the thermodynamic model, the Gibbs energy of ternary liquid solution was interpolated using the ‘Toop’ type interpolation technique from the binary system. ‘Toop’ technique was selected based on the nature of three binary systems. Then two small ternary model parameters were added to reproduce the available phase diagram data accurately. No new ternary compounds or ternary extensions of binary compounds were considered in this study because no such information was reported. The review of experimental studies and the comparison of the optimization results with experimental data are presented below.

Three experimental studies focused on the expansion of the liquid miscibility gap of the Ca-Fe system to the ternary Ca-Fe-Si system. The experiments were carried out under a high-purity Ar gas atmosphere due to the strong oxidation behavior of Ca and special attention was taken to prevent the evaporation of Ca during melting and isothermal holding. The miscibility gap in the Fe-Ca rich corner at 1873 K (1600 °C) was investigated by Golev and Belyaev^[39] using a graphite crucible at 1 bar in Ar gas and by Köhler *et al.*^[37] using a dense CaO crucible at 10 bar in Ar gas. Ototani and Kataura^[35] also investigated the miscibility gap in the ternary system but the temperature of the experiments was not well specified in their paper: from the discussion

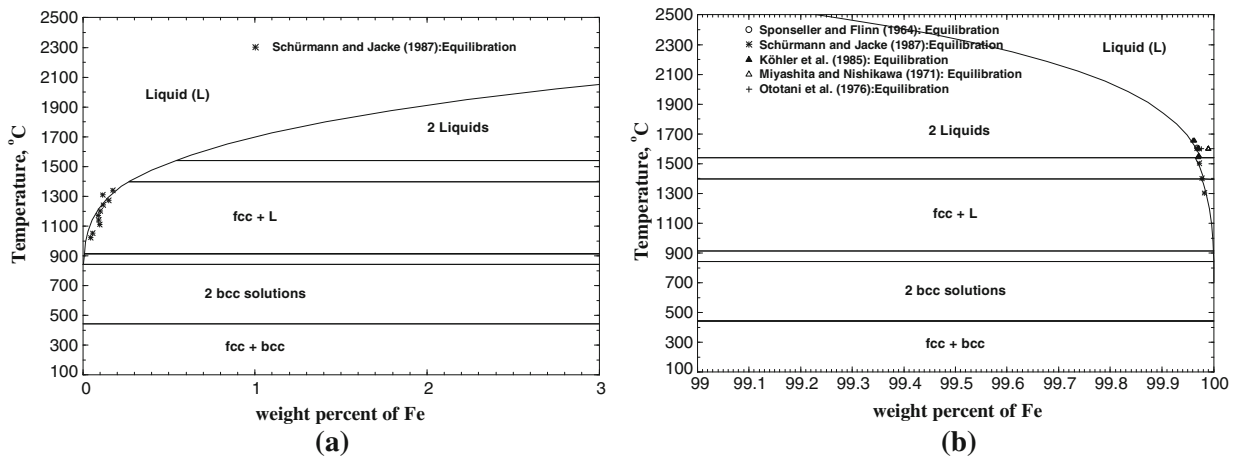


Fig. 6—Calculated phase diagrams in (a) Ca-rich side and (b) Fe-rich side of the Ca-Fe system.

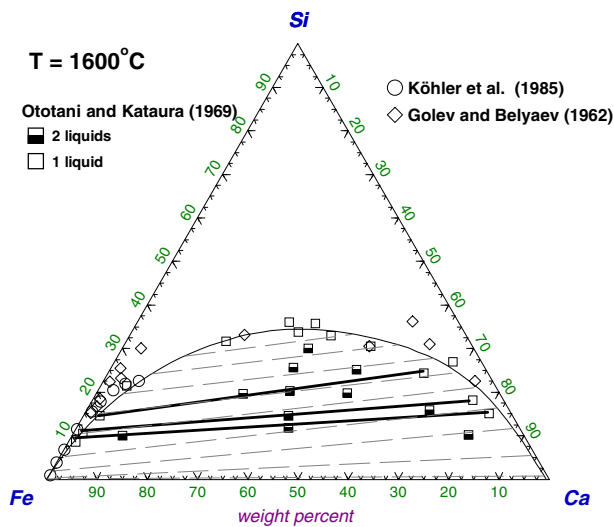


Fig. 7—Phase diagram of the Ca-Fe-Si system calculated at 1873 K (1600 °C).

in their paper, it should be above 1673 K (1400 °C) (In this study, we assumed the experimental temperature of the work by Ototani and Kataura is 1873 K (1600 °C)). All the experimental data are plotted in Figure 7. Although there is scatter in the experimental data, in particular in the Ca-rich region, the agreement is quite good considering the experimental difficulty in determining the miscibility gap. The Modified Quasichemical Model with only binary parameters predicts the liquid miscibility gap of larger solubility of Ca in the Fe-rich region and smaller solubility of Fe in the Ca-rich region than experimental data. Ternary model parameters are required to modify the shape of miscibility gap. This is rather unusual from the authors' experience. With the use of two ternary liquid parameters, the experimental liquid miscibility gap is well reproduced as shown in Figure 7. It should be noted that the size of liquid miscibility gap does not change significantly between 1673 K and 1873 K (1400 °C and 1600 °C). The previous thermodynamic assessment by Anglèzio *et al.*^[4] shows a much larger miscibility gap than the experi-

mental results, shown in Figure 7. Their miscibility gap expanded up to about 40 wt pct Si at 1873 K (1600 °C) and two liquid miscibility gaps were calculated at 1623 K (1350 °C) which seems unlikely in this ternary system.

The Si-rich corner (wt pct Si >40) of the Fe-Ca-Si system was investigated by Schürmann *et al.*^[40] using thermal analysis and optical microscopic analysis of solidified samples. In total, 45 samples (in many samples, total impurity of Al and C reached 1 wt pct) were prepared in the ternary system for thermal analysis, but the choice of alloy composition was seemingly random and therefore the complete phase diagram for any specific pseudo-binary section or isopleth can not be made from the experimental results. In the present study, the predicted liquidus from the Modified Quasichemical Model without any ternary parameters is lower than experimental data in the middle and high Si region, parameters were added to reproduce the liquidus. Two isoplethes of the Ca-Fe-Si system are calculated in Figure 8 and compared with experimental data. In the case of the isopleth at 48 wt pct Si, the calculated liquidus in the high Fe region is noticeably lower than the experimental data. However, the experimental data at this region are not consistent with binary experimental data. The liquidus of the isopleth at 60 wt pct Si is also lower than the experimental data at 10 to 15 wt pct Fe (liquidus of FeSi), which can be significantly increased with a slight decreasing Si content. In general, the agreement between the calculated phase diagram and experimental data is good with the consideration of possible experimental error (compositional change of starting alloy during the experiment).

Schürmann *et al.*^[40] speculated the possible phase diagram of the Ca-Fe-Si system in the Fe-rich corner from the liquid miscibility gap experimental data of Golev and Belyaev^[39] and Ototani and Kataura.^[35] Figure 9(a) shows the calculated liquidus projection in the Fe-rich corner of the Ca-Fe-Si system from the present thermodynamic modeling. A large miscibility gap area can be calculated. In particular, the primary crystallization regions of Ca₂Si and Ca₅Si₃ are predicted in the Fe-rich corner along the liquid miscibility gap

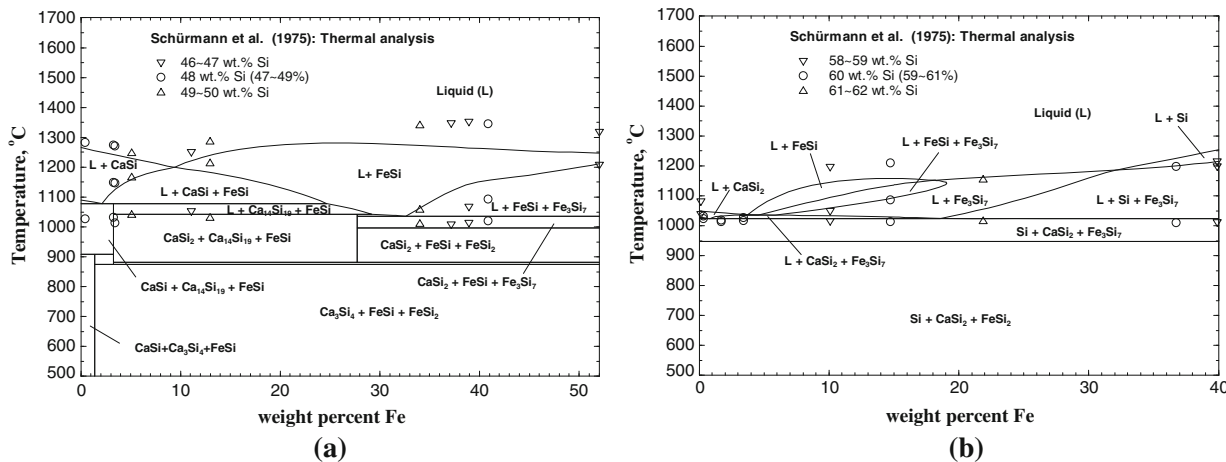


Fig. 8—Calculated isopleths of the Ca-Fe-Si system along with the experimental data of Schürmann *et al.*^[33] (a) 48 wt pct Si and (b) 60 wt pct Si.

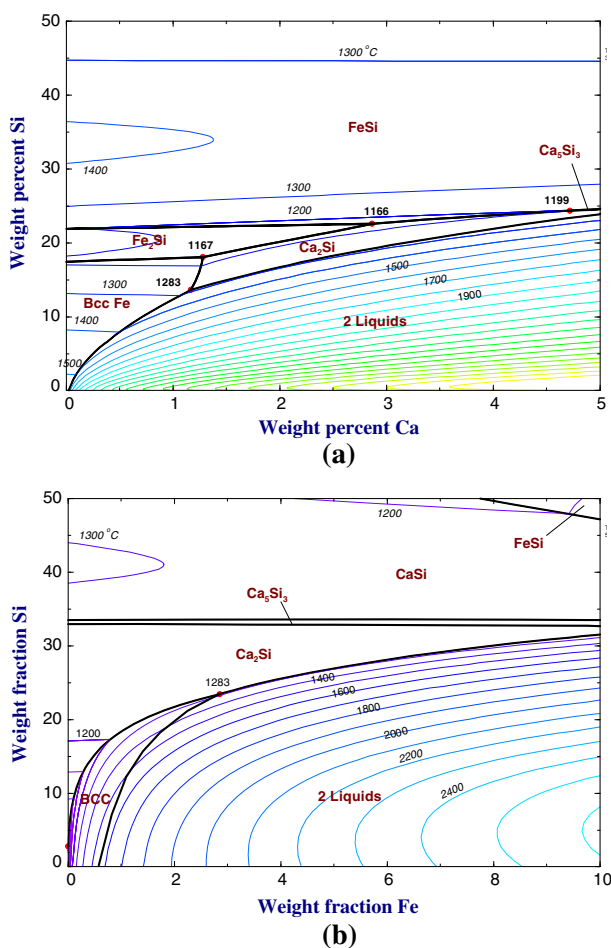


Fig. 9—Calculated liquidus projections at (a) Fe-rich corner and (b) Ca-rich corner of the Ca-Fe-Si system.

because these phases are forming along a miscibility gap in the Ca-rich corner. Although Schürmann *et al.*^[40] speculated the possible primary crystallization region of

CaSi in Fe-rich corner, this is not calculated in the present diagram because the primary crystalline region of CaSi phase does not touch the miscibility region in the Ca-rich side, as shown in Figure 9(b). The formation of a Ca-rich phase during the solidification of Fe-rich alloys is an interesting feature due to a large liquid miscibility gap.

Using the optimized model parameters in the present study, any phase diagram of the Ca-Fe-Si system can be calculated. The phase stability diagram of the Ca-Fe-Si system at 673 K (400 °C) is calculated in Figure 10(a) and the phase diagrams for the CaSi-FeSi and CaSi₂-FeSi₂ sections are calculated in Figures 10(b) and (c), respectively. In the case of the pseudo-binary CaSi-FeSi system, a liquid miscibility gap is predicted to exist in this join, which results from the large miscibility gap shown in Figure 7. The predicted liquidus projection for the entire Ca-Fe-Si system is presented in Figure 11.

As mentioned earlier, the experimental phase diagram information is still very limited. It is possible to have limited mutual solid solutions between Ca_xSi_y and Fe_xSi_y compounds. However, from the solid state miscibility gap between bcc and fcc Ca-Fe solutions, it is expected that the mutual solubility will be very small. The existence of ternary phases has not been well investigated and therefore requires more examination.

IV. APPLICATION TO THE SI-REFINING PROCESS: FE REMOVAL IN THE ACID-LEACHING PROCESS

As Fe is difficult to remove from molten Si using typical slag-refining techniques, an acid-leaching process has been proposed as a promising processing route for the removal of Fe from metallurgical grade Si (MG-Si). As can be seen in Figures 2 and 4, the solubilities of Ca and Fe in solid Si (Diamond_A4) are very small. Most of Ca and Fe impurities in molten Si therefore can be precipitated on the dendritic boundaries of Si during the solidification process. Various concentrations of

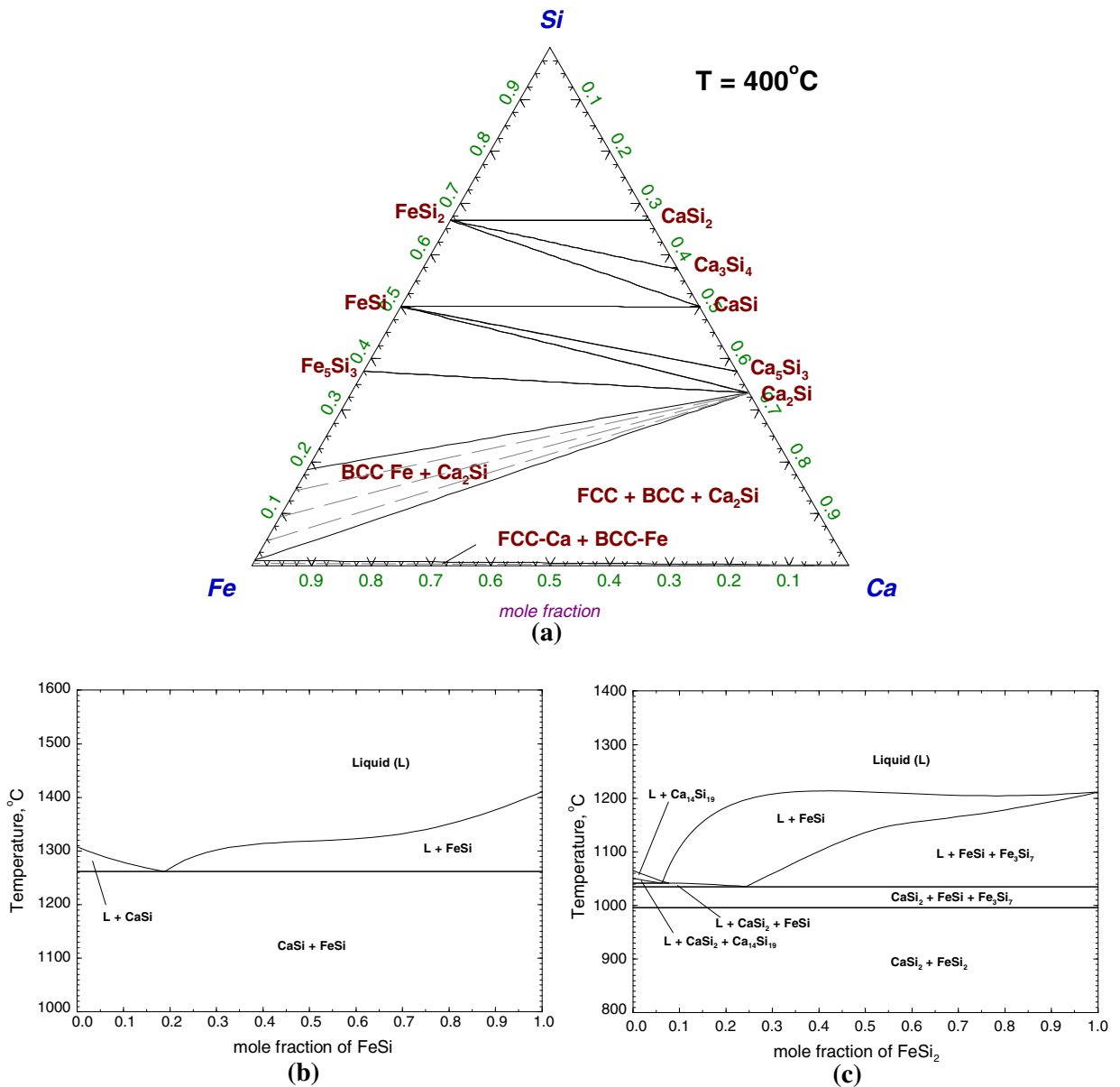


Fig. 10—Calculated phase diagrams of the Ca-Fe-Si system from the present thermodynamic modeling. (a) Isothermal section at 673 K (400 °C), (b) pseudo-binary phase diagram of the CaSi-FeSi system, and (c) isopleth of the CaSi_2 - FeSi_2 section.

leaching agents (HNO_3 , H_2SO_4 , HCl , and HF) and temperature can be used in acid-leaching process. The refining capacity of metallurgical Si can be dependent on the composition of agents and temperature. For example, HCl solution is less effective to remove Fe-Si compound than HF solution.^[41]

One of the interesting studies for the acid leaching of MG-Si using HCl solution was carried out by Sakata *et al.*^[3] They found a relationship between the ratio of Ca to Fe concentration and the removal ratio of Ca and Fe during the acid-leaching process with HCl solution of solidified high-purity Si-Ca-Fe alloys. The removal rate of Fe increases with $X_{\text{Ca}}/X_{\text{Fe}}$ ratio and reaches a maximum when $X_{\text{Ca}}/X_{\text{Fe}} > \sim 10$. On the other hand, the Ca removal rate depends less on the $X_{\text{Ca}}/X_{\text{Fe}}$ ratio in Si alloys. This was explained by Morita and Miki^[2] from

the solidified microstructure of Si alloys. In the acid-leaching process using HCl solution, Ca (CaSi_2) is soluble in acid solutions, while FeSi_2 is non-soluble. In Si alloys with high $X_{\text{Ca}}/X_{\text{Fe}}$ ratios, CaSi_2 is formed as a secondary solid phase along the dendrite boundaries of the primary Si phase. The remaining Fe in molten Si can then be precipitated at the end of the solidification process as a eutectic phase embedded in CaSi_2 . Consequently, during the dissolution of CaSi_2 in the acid-leaching process, eutectic FeSi_2 particles can be physically separated from the Si dendrites to increase the removal rate of Fe from Si. On the other hand, Si alloys with low Ca/Fe ratios can produce FeSi_2 as a secondary phase directly segregated on the dendritic boundaries of the primary Si phase, which are difficult to remove during the acid-leaching process. Of course, the cooling

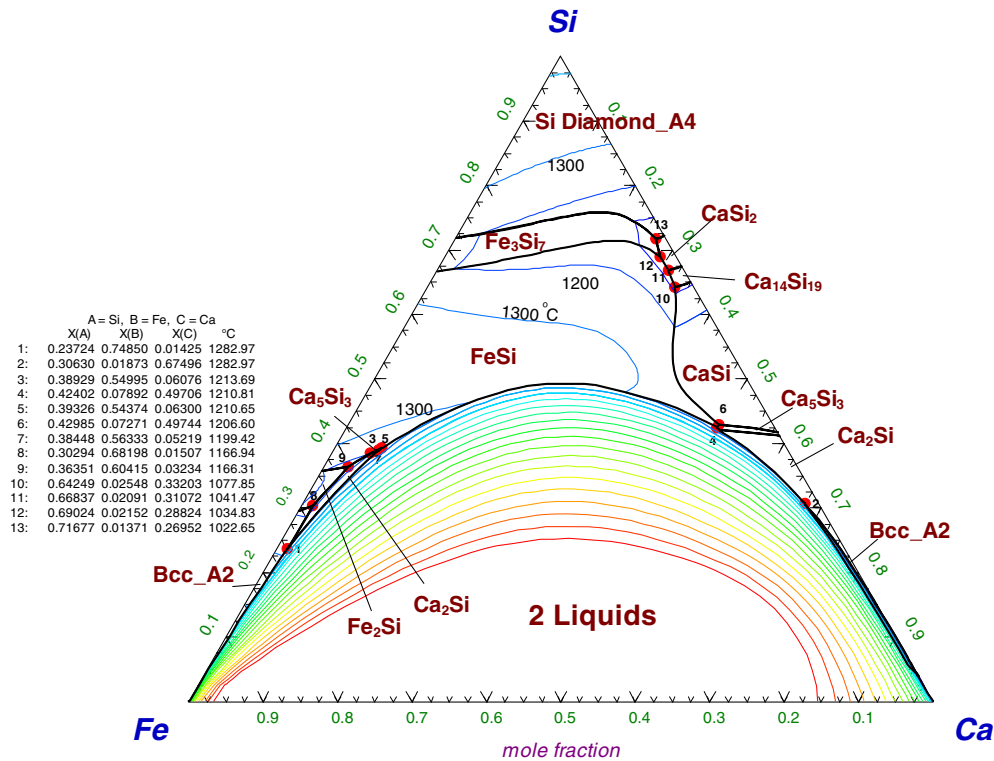


Fig. 11—Calculated liquidus projection of the Ca-Fe-Si system.

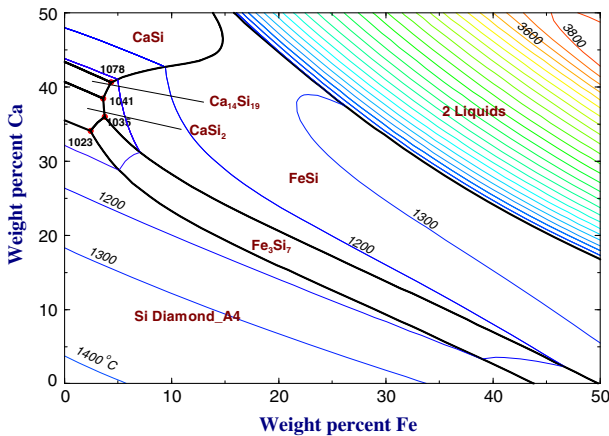


Fig. 12—Calculated liquidus projection of the Si-rich region of the Si-Ca-Fe system.

rate of molten Si alloys during solidification can also affect the microstructure development and change the removal rates of Fe and Ca.

The liquidus projection in the Si-rich corner of the Ca-Fe-Si system is shown in Figure 12. According to these calculations, CaSi_2 or Fe_3Si_7 can be produced as secondary phases during the solidification of Si-rich liquid alloys depending on the Ca/Fe ratio; moreover, the final eutectic structure ($L \rightarrow \text{Si} + \text{CaSi}_2 + \text{Fe}_3\text{Si}_7$) can occur at 1296 K (1023 °C). The molar ratio Ca/Fe of the eutectics is calculated to be 19.7. That is, when the molar Ca/Fe ratio is higher than 19.7, CaSi_2 can be

formed as a secondary phase and when the ratio is lower than 19.7, Fe_3Si_7 can be formed as a secondary phase. According to the equilibrium phase diagram, FeSi_2 cannot be formed. Consequently, Sakata *et al.*^[3] may have taken Fe_3Si_7 for FeSi_2 in their study or Fe_3Si_7 dissociated into FeSi_2 plus Si due to the eutectoid reaction at 1221 K (948 °C) after solidification (see Figure 3).

In fact, Fe_3Si_7 (or sometime called as Fe_2Si_5) phase is known as high-temperature FeSi_2 ($\text{FeSi}_{2.4}$ or α -leboite). According to the early study by Anglézio *et al.*,^[42] Fe_3Si_7 was found in the solidification microstructure of MG-Si. However, recent study by Meteleva-Fischer *et al.*,^[43] low-temperature FeSi_2 (β - FeSi_2) containing several percent of Al was observed in the solidified MG-Si with addition of 5 to 6 wt pct of Ca. Recent phase diagram study of the Al-Fe-Si system by Marker *et al.*^[44] shows that both high (α -) and low (β -) temperature FeSi_2 can be further stabilized by Al as solid solutions. Therefore, it seems that different crystal phases of FeSi_2 can be formed depending on the real chemistry of MG-Si. In the present study, we assumed that Fe_3Si_7 (α -leboite) as FeSi_2 crystal phase according to the thermodynamic relationship in the Si-Fe-Ca system.

As is well known, Scheil cooling calculations (assuming no diffusion in the solid state and complete diffusion in the liquid state during solidification) can provide relatively good predictions of as-cast microstructures. Variations in the amounts of secondary and eutectic phases in the as-cast microstructures of Si-Ca-Fe alloys can be evaluated using Scheil cooling calculations. Scheil

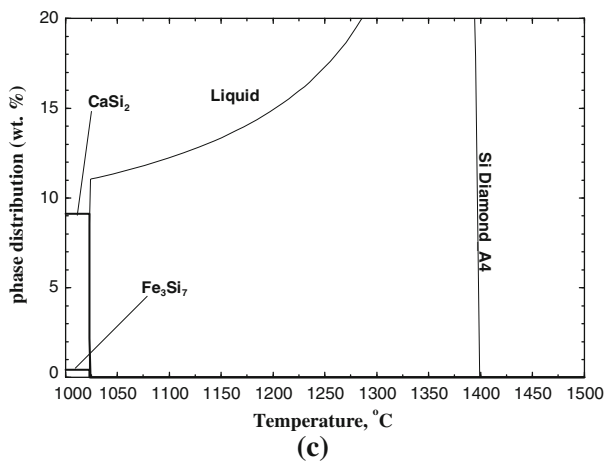
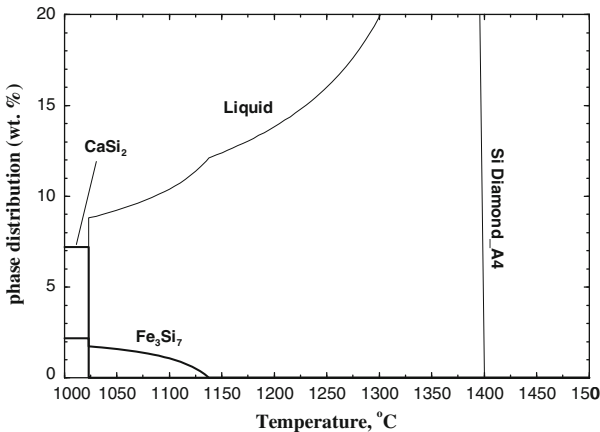
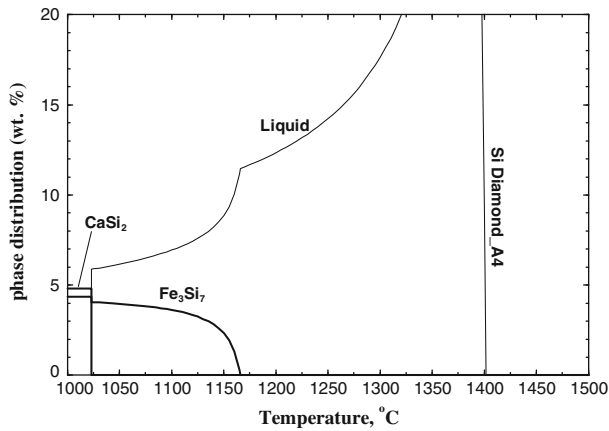


Fig. 13—Scheil cooling calculations for various Si-Ca-Fe alloys. (a) Si-2Ca-2Fe, (b) Si-3Ca-1Fe, and (c) Si-3.8Ca-0.2Fe (wt pct).

cooling results for Si-Ca-Fe alloys using the present thermodynamic database are depicted in Figures 13 and 14. In order to determine the effect of the Ca/Fe ratio on the secondary and eutectic solid phases, calculations were performed with molten Si containing a total 4 wt pct impurities (wt pct Ca + wt pct Fe = 4.0) and by varying the Ca content from 0.1 to 3.9 wt pct Ca.

The changes in phase distributions of three Si alloys with temperature are presented in Figure 13: (a) Si-2Ca-2Fe,

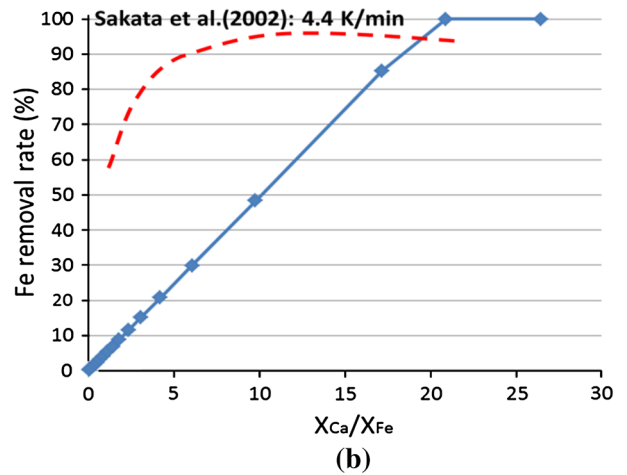
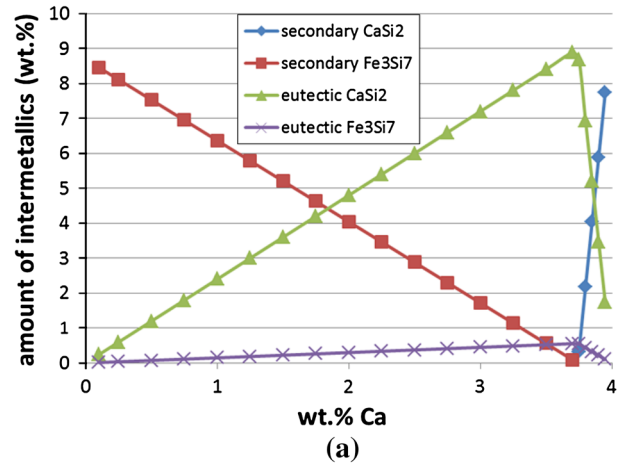


Fig. 14—Evolution of secondary and eutectic phases from the Scheil cooling calculation for the Si-Ca-Fe alloys (impurity Ca + Fe = 4 wt pct). (a) Variation of the amount of secondary and eutectic phases with Ca content in alloy and (b) theoretical Fe removal rate with molar ratio of Ca/Fe in molten Si along with the experimental results from Sakata *et al.*^[3].

(b) Si-3Ca-1Fe, and (c) Si-3.8Ca-0.2Fe (in wt pct). For the equivalent amount of Ca and Fe impurity in molten Si (Si-2Ca-2Fe), a large amount of Fe₃Si₇ forms as a secondary phase in between Si dendrites from 1443 K (1170 °C). Then, an additional small amount of Fe₃Si₇ phase forms at 1296 K (1023 °C) as a eutectic phase. In this alloy, CaSi₂ forms only as a eutectic phase and the amount is 4.8 wt pct, which is slightly larger than the total amount of Fe₃Si₇ (4.35 wt pct). In the case of a Si-3Ca-1Fe alloy, although Fe₃Si₇ forms as a secondary phase, the amount of CaSi₂ is about three times larger than that of Fe₃Si₇ in term of total segregation. The calculations for the Si-3.8Ca-0.2Si alloy show that CaSi₂ can form first as a secondary phase just above the eutectic temperature and then most precipitates form as a eutectic mixture of CaSi₂ and Fe₃Si₇.

The predicted amounts of secondary and eutectic phases from the Scheil cooling calculations are summarized in Figure 14. As can be seen in Figure 14(a), the amount of secondary Fe₃Si₇ is linearly decreasing with increasing Ca content in Si alloy until 3.7 wt pct Ca. The amount of eutectic CaSi₂ phase linearly increases

and drastically decreases after 3.7 wt pct Ca and instead secondary CaSi_2 phase forms after 3.7 wt pct Ca. It is interesting to note that eutectic Fe_3Si_7 increases until 3.7 wt pct Ca and decreases thereafter. If we assume, following the idea of Morita and Miki,^[2] that eutectic Fe_3Si_7 can be easily removed during the dissolution of CaSi_2 in acid-leaching process and secondary Fe_3Si_7 phase cannot be removed in this process, the theoretical removal rate of Fe can be calculated as

$$\begin{aligned} &\text{Theoretical removal rate of Fe} \\ &= \frac{\text{Amount of secondary } \text{Fe}_3\text{Si}_7}{\text{Total segregation amount of } \text{Fe}_3\text{Si}_7}. \end{aligned} \quad [16]$$

The evaluated theoretical removal rate is presented in Figure 14(b). The removal rate is linearly increasing with Ca/Fe molar ratio. In comparison to the experimental results of Sakata *et al.*,^[3] the calculated removal rate is much lower at given Ca/Fe ratio. This discrepancy can be reduced if we consider that part of secondary Fe_3Si_7 phase can be removed by (i) physical detachment during mechanical crashing of solidified Si and (ii) partial detachment of secondary Fe_3Si_7 in between eutectic phases during the dissolution of CaSi_2 during the acid-leaching process. The exact contributions of these aspects are difficult to estimate, there could be other contributions.

According to the results of Sakata *et al.*,^[3] the removal rates of Fe and Ca depend on the cooling rate, which could change the as-cast microstructure of Si alloys. The cooling rate can modify the following aspects of the as-cast microstructure: primary Si dendrite size, secondary dendrite arm spacing of Si dendrites, and size distribution of precipitates in between Si dendrites. The microsegregation of solute Fe and Ca in Si dendrites and total amount of Fe_3Si_7 and CaSi_2 precipitates are less sensitive to the cooling rate in conventional cooling conditions because the maximum solubility of Fe and Ca in solid Si is very low. Therefore, the smaller dendrites formed at higher cooling rates can result in smaller precipitations in between Si dendrites, which makes them difficult to detach during mechanical crashing and to be dissolved during the acid-leaching process. In fact, according to Sakata *et al.*, the removal rate of Fe and Ca in quenched samples is about 10 to 20 pct lower than slow-cooled samples.

In summary, the phase diagram information can provide guidelines for the removal rate of Fe in MG-Si during the acid-leaching process by providing the amount of secondary and eutectic precipitates of Fe_3Si_7 and CaSi_2 phases in cast alloys. However, the removal rate of Fe seems to be highly dependent on the distribution of precipitates in as-cast microstructure as well as the amount of precipitates.

V. SUMMARY

Accurate thermodynamic and phase diagram data for the Ca-Fe-Si system are required in order to understand the as-cast microstructure evolution during the acid-

leaching refining process to produce metallurgical grade Si. In order to meet this need, a thermodynamic optimization of the binary Ca-Fe and ternary Ca-Fe-Si systems has been conducted based on the critical evaluation of all available phase diagram and thermodynamic properties data available. The thermodynamic properties of liquid solutions were described using the Modified Quasichemical Model to take into account the SRO in the liquid state. A thermodynamic database containing a set of model parameters for all solid and liquid phases was produced, which allows for the calculation of any phase diagram section of any binary and ternary system in conjunction with a Gibbs energy minimization routine, such as the FactSage system. Several phase diagrams of pseudo-binary sections and isopleths in the ternary Ca-Fe-Si system are predicted from the present thermodynamic database. The liquidus projection of the ternary system is also predicted. The thermodynamic database is also applied to the metallurgical grade Si-refining process. The theoretical Fe removal rate of solidified Si-Ca-Fe alloys was calculated for an acid-leaching process based on the Scheil cooling calculation results. The discrepancy between the model and experimental results was discussed.

ACKNOWLEDGMENTS

The present work was financially supported by NSERC-Automotive Partnership Canada program in Canada.

REFERENCES

1. K. Tang, E.J. Oevrelid, G. Tranell, and M. Tangstad: *Adv. Mater. Res.*, 2009, vol. 14, pp. 219–51.
2. K. Morita and T. Miki: *Intermetallics*, 2003, vol. 11, pp. 1111–17.
3. T. Sakata, T. Miki, and K. Morita: *Nippon Kinzoku Gakkaishi*, 2002, vol. 66, pp. 459–65.
4. J.C. Anglézio, C. Servant, and I. Ansara: *CALPHAD*, 1994, vol. 18, pp. 273–309.
5. C.W. Bale, E. Béglise, P. Chartrand, S.A. Degterov, G. Eriksson, K. Hack, I.H. Jung, Y.B. Kang, J. Melançon, A.D. Pelton, C. Robelin, and S. Petersen: *CALPHAD*, 2009, vol. 33, pp. 295–311.
6. G. Inden: *Project Meeting Calphad V*, Max-Planck-Institut für Eisenforschung G.m.b.H., Dusseldorf, Germany, 1976, pp. 111.
7. M. Hillert and M. Jarl: *CALPHAD*, 1978, vol. 2, pp. 227–38.
8. A.D. Pelton and P. Chartrand: *Metall. Mater. Trans. A*, 2001, vol. 32A, pp. 1355–60.
9. A.D. Pelton, S.A. Degterov, G. Eriksson, C. Robelin, and Y. Dessureault: *Metall. Mater. Trans. B*, 2000, vol. 31B, pp. 651–59.
10. M. Heyrman and P. Chartrand: *J. Phase Equilib. Diffus.*, 2006, vol. 27, pp. 220–30.
11. S. Cui and I.-H. Jung: Unpublished research, 2013.
12. I.-H. Jung, D.H. Kang, W.J. Park, N.J. Kim, and S. Ahn: *CALPHAD*, 2007, vol. 31, pp. 192–200.
13. D. Nassyrov and I.H. Jung: *CALPHAD*, 2009, vol. 33, pp. 521–29.
14. A.D. Pelton and M. Blander: *Metall. Trans. B*, 1986, vol. 17, pp. 805–15.
15. P. Wu, G. Eriksson, A.D. Pelton, and M. Blander: *ISIJ Int.*, 1993, vol. 33, pp. 26–35.
16. L. Kaufman, B. Uhrenius, D. Birnie, and K. Taylor: *CALPHAD*, 1984, vol. 8, pp. 25–66.
17. A.D. Pelton: *CALPHAD*, 2001, vol. 25, pp. 319–28.
18. K. Frisk and M. Selleby: *J. Alloys Compd.*, 2001, vol. 320, pp. 177–88.

19. H. Sigmund: *J. Electrochem. Soc.*, 1982, vol. 129, pp. 2809–12.
20. J. Lacaze and B. Sundman: *Metall. Trans. A*, 1991, vol. 22A, pp. 2211–23.
21. K. Tang and M. Tangstad: *Acta Metall. Sin.*, 2012, vol. 25, pp. 249–55.
22. A.A. Istratov, H. Hieslmair, and E.R. Weber: *Appl. Phys. A Mater. Sci. Process.*, 1999, vol. 69, pp. 13–44.
23. F.A. Trumbore: *Bell Syst. Tech. J.*, 1960, vol. 30, pp. 205–23.
24. H. Feichtinger: *Acta Phys. Austriaca*, 1979, vol. 51, pp. 161–84.
25. Y.H. Lee, R.L. Kleinhenz, and J.W. Corbett: *Appl. Phys. Lett.*, 1977, vol. 31, pp. 142–44.
26. S.A. McHugo, R.J. McDonald, A.R. Smith, D.L. Hurley, and E.R. Weber: *Appl. Phys. Lett.*, 1998, vol. 73, pp. 1424–26.
27. E.G. Colas and E.R. Weber: *Appl. Phys. Lett.*, 1986, vol. 48, pp. 1371–73.
28. J.D. Struthers: *J. Appl. Phys.*, 1956, vol. 27, p. 1560.
29. H. Nakashima, T. Isobe, Y. Yamamoto, and K. Hashimoto: *Jpn J. Appl. Phys.*, 1988, vol. 27, pp. 1542–43.
30. D. Gilles, W. Schroeter, and W. Bergholz: *Phys. Rev. B*, 1990, vol. 41, pp. 5770–82.
31. E. Weber and H.G. Riottte: *J. Appl. Phys.*, 1980, vol. 51, pp. 1484–88.
32. N. Wiehl, U. Herpers, and E. Weber: *J. Radioanal. Chem.*, 1982, vol. 72, pp. 69–78.
33. E. Schürmann and H. Jacke: *Steel Res.*, 1987, vol. 58, pp. 399–405.
34. D.L. Sponseller and R.A. Flinn: *Trans. Am. Inst. Min. Metall. Pet. Eng.*, 1964, vol. 230, pp. 876–88.
35. T. Ototani and Y. Kataura: *Nippon Kinzoku Gakkaishi*, 1968, vol. 32, pp. 458–63.
36. Y. Miyashita and K. Nishikawa: *Tetsu to Hagane*, 1971, vol. 57, pp. 1969–75.
37. M. Köhler, H.J. Engell, and D. Janke: *Steel Res.*, 1985, vol. 56, pp. 419–23.
38. H. Okamoto: *J. Phase Equilib. Diffus.*, 2010, vol. 31, pp. 88–90.
39. A.K. Golev and G.S. Belyaev: *Izv. Akad. Nauk SSSR Otd. Tekh. Nauk, Metall. Topl.*, 1962, pp. 114–15.
40. E. Schürmann, H. Litterscheidt, and P. Fuenders: *Arch. Eisenhüttenwes.*, 1975, vol. 46, pp. 427–32.
41. I.C. Santos, A.P. Goncalves, C.S. Santos, M. Almeida, M.H. Afonso, and M.J. Cruz: *Hydrometallurgy*, 1990, vol. 23, pp. 237–46.
42. J.C. Anglèzio, C. Servant, and F. Dubrous: *J. Mater. Res.*, 1990, vol. 5, pp. 1894–99.
43. Y.V. Meteleva-Fischer, Y. Yang, R. Boom, B. Kraaijveld, and H. Kuntzel: *Intermetallics*, 2012, vol. 25, pp. 9–17.
44. M.C.J. Marker, B. Skolyszewska-Kühberger, H.S. Effenberger, C. Schmetterer, and K.W. Richter: *Intermetallics*, 2011, vol. 19, pp. 1919–29.